Carbohydrate Polymers 229 (2020) 115498

Contents lists available at ScienceDirect

Carbohydrate Polymers

journal homepage: www.elsevier.com/locate/carbpol

Anisamide-functionalized pH-responsive amphiphilic chitosan-based paclitaxel micelles for sigma-1 receptor targeted prostate cancer treatment

Ding Qu[a,b,1], Mengying Jiao[a,1], Haijiao Lin[a], Chunli Tian[a], Guowei Qu[a], Jingwei Xue[a], Lingjing Xue[a], Caoyun Ju[a,*], Can Zhang[a,*]

[a] State Key Laboratory of Natural Medicines, Jiangsu Key Laboratory of Drug Discovery for Metabolic Diseases, Center of Advanced Pharmaceuticals and Biomaterials, China Pharmaceutical University, Nanjing 210009, PR China

[b] Affiliated Hospital of Integrated Traditional Chinese and Western Medicine, Nanjing University of Chinese Medicine, Nanjing 210028, PR China

ARTICLE INFO

Keywords:
Amphiphilic chitosan derivate
Micelles
Prostate tumor targeting
pH-responsive release
Paclitaxel

ABSTRACT

Controlled release and tumor-selective distribution are highly desirable for anticancer nanomedicines. Here, we design and synthesize an anisamide-conjugated *N*-octyl-*N,O*-maleoyl-*O*-phosphoryl chitosan (a-OMPC) which can form amphiphilic micelles featuring pH-responsive release and high affinity to sigma-1 receptor-overexpressed tumors for paclitaxel (PTX) delivery. Thereinto, maleoyl and phosphoryl groups cooperatively contribute to pH-responsive drug release due to a conversion from hydrophile to hydrophobe in the acidic microenvironment of endo/lysosomes. We demonstrated that PTX-loaded a-OMPC micelles (PTX-aM) enhanced the cellular internalization *via* the affinity between anisamide and sigma-1 receptor, rapidly released drug in endo/lysosomes and elevated the cytotoxicity against PC-3 cells. The in vivo studies further verified that PTX-aM could largely accumulate at the tumor site even after 24 h of administration, resulting in obvious inhibition effect and prolonged survival period in PC-3 tumor xenograft-bearing mice. Moreover, OMPC showed no obvious hemolytic and acute toxicity. Collectively, this chitosan derivate holds a promising potential in application of prostate cancer-targeted drug delivery system.

1. Introduction

Prostate cancer (PCa) is one of the most commonly diagnosed male-related diseases in western countries, accounting for about 70% incidence worldwide (Allemani et al., 2018). In the past 5 years, the PCa population in China dramatically increased, which was associated with the changes in lifestyle, living environment and work pressure (Kimura & Egawa, 2018; Wu et al., 2015). Although the 5-year survival rate of PCa patients is high as 98.9% in part due to the advanced early diagnostic techniques in western countries (Allemani et al., 2018; DeSantis et al., 2014; Wu et al., 2015), China's 5-year survival rate is only 50–60%, presenting major challenges in effective treatment (Allemani et al., 2018; DeSantis et al., 2014). In addition to surgical operation and radiotherapy, chemotherapy such as paclitaxel (PTX) is still a primary remedy in the treatment of PCa, especially for androgen receptor-negative patients who have created tolerance to antiandrogen therapy (Saari et al., 2015; Thomas et al., 2017; Yang, Mondal et al., 2017). However, due to lack of tumor-targeted ability, severe side effects of PTX depress the patients' compliance and diminish their quality of life.

Targeted drug delivery technology can deliver enough therapeutic agent to the desired sites, and thereby of reducing the systemic toxicity and enhancing the treatment efficacy (Chen et al., 2018; Huang et al., 2017; Liu et al., 2018; Wang, Zhu, Liu, Dong, & Liu, 2018). As reported previously, certain receptors differ in expression on the surface of tumor cells and normal cells, which is considered as a potential strategy to endow nanomedicine with active tumor-specific targeting (Jhaveri, Deshpande, Pattni, & Torchilin, 2018). Sigma-1 receptor, required for prostate cancer cell growth and survival, is observed overexpressed in several types of human prostate tumor cells (Dasargyri, Kümin, & Leroux, 2017; Urandur et al., 2018; Yang, Comeau et al., 2017). As a membrane-binding protein, sigma-1 receptor has high affinity to small molecules, such as anisamide which has been conjugated to PEGylated gold nanorods loading epirubicin for targeted chemo-photothermal therapy in PC-3 tumor xenograft-bearing mice (Evans et al., 2017; Wang et al., 2019).

Chitosan, as the unique natural polysaccharide with positive charge (Bhattarai, Gunn, & Zhang, 2010; Buschmann et al., 2013; Castro et al., 2017; Ruetz & Gros, 1995), is identified as a promising backbone for

* Corresponding authors.
E-mail addresses: jucaoyun@cpu.edu.cn (C. Ju), zhangcan@cpu.edu.cn (C. Zhang).

[1] Authors contributed equally to this work.

https://doi.org/10.1016/j.carbpol.2019.115498
Received 17 June 2019; Received in revised form 3 September 2019; Accepted 17 October 2019
Available online 21 October 2019
0144-8617/

amphiphilic polymer due to its distinctive biology characteristics. In our previous studies, we have synthesized *N*-octyl-*O*-sulfate chitosan (NOSC) (Jin, Mo, Ding, Zheng, & Zhang, 2014; Mo et al., 2011), *N*-octyl-*N*-phthalyl-3,6-*O*-(2-hydroxypropyl) chitosan (OPHPC) (Qu, Lin, Zhang, Xue, & Zhang, 2013), *N*-octyl-*N,O*-succinyl-*O*-phosphoryl chitosan (OSPC) (Zhang et al., 2016), *N*-octyl-*N*'-phthalyl-*O*-phosphate chitosan (OPPC) (Qu et al., 2019), and so on. Such designed amphiphilic chitosan derivatives are able to self-assemble into polymer micelles with impressive capacity of solubilization to various chemotherapeutic agents, and thereby of enhancing anticancer efficacy to some extent. To further improve the anticancer efficacy, it is optional to endow these chitosan derivatives with tumor targeting or stimuli-triggered drug release ability. However, it is challenging to prepare multifunctional amphiphilic chitosan with high drug-loading capacity due to lack of enough chemically-active sites of chitosan being utilized for amphiphilic modification.

Herein, we designed and synthesized an anisamide-conjugated *N*-octyl-*N,O*-maleoyl -*O*-phosphoryl chitosan derivative (a-OMPC) with tumor targeting ability and pH sensitivity for controlled drug delivery. Of which, phosphoryl as hydrophilic group and octyl as hydrophobic group maintain a basic amphiphilic chitosan structure. The modification with maleoyl groups enables chitosan to gain a distinctive solubility in organic system. Moreover, maleoyl unit provides α,β-unsaturated ketone double bond for the conjugation of anisamide, which will offer the chitosan derivative a high affinity to sigma-1 receptor overexpressed on the surface of PCa cells. In addition, owing to the conversion from hydrophilic phosphate/carboxylate to hydrophobic phosphoric acid/carboxylic acid at the endo/lysosomal pH, simultaneous introduction of maleoyl and phosphoryl group enables a-OMPC to regulate the solubility in aqueous and organic system as pH changes, and thereby of releasing drug in a pH-responsive manner (Scheme 1A). Based on improved characteristics, we fabricated a PTX-loaded a-OMPC micelle system (PTX-aM) featuring pH-responsive release and PCa targeting. As our hypothesis, PTX-aM could accumulate in the vicinity of tumor sites by the EPR effect and recognize the tumor cells through the anisamide-sigma receptor affinity. After endocytosis of human prostate tumor (PC-3) cells, micelles are entrapped by lysosomes, resulting in rapid drug release and thereby of enhancing the anti-tumor efficacy (Scheme 1B). This study focuses on the synthesis and characterization of chitosan derivative, preparation of PTX-loaded micelles, intracellular stability and delivery, tumor targeting and anticancer efficacy to validate the rationality and potential of PTX-aM in PCa treatment. Moreover, we also evaluate the biocompatibility of a-OMPC for future application.

2. Materials and methods

2.1. Materials

Chitosan was purchased from Haidebei Biochemical Co., Ltd. (Shandong, China), with a deacetylation degree of 92% and viscosity average molecular weight of 70 kDa. PTX (purity > 99.9%) was obtained from Yew Pharmaceutical Co., Ltd. (Jiangsu, China). Taxol® was purchased from Shanghai Squibb Pharmaceutical Co., Ltd. Cremophor® EL was a generous gift from BSAF (Germany). Octanal, maleic anhydride, polyphosphoric acid (PPA), pyrene, *N*-(*p*-anisoyl) cysteine, L-cysteine and 1*H*-benzotriazole were bought from Sinopharma group Co., Ltd. (Shanghai, China). 3-(4,5-dimethylthiazol-2-yl)-2,5-iphenyltetrazolium bromide (MTT), fluorescein isothiocyanate (FITC), 1,1′,3,3,3′,3′-hexamethylindo dicarbocyanine iodide (DiI), 3,3′-dioctadecyloxacarbocyanine perchlorate, 3,3′-dioctadecyloxacarbocyanine perchlorate (DiO), 1,1-dioctadecyl-3,3,3,3-tetramethylin-dodicarbo cyanine iodide (DiD) were purchased from Aladdin Chemical Co., Ltd. (Shanghai, China). RPMI-1640 medium, Ham's F-12 medium, fetal bovine serum (FBS), penicillin-streptomycin solution, BCA protein assay kit and phosphate buffered saline (PBS) were purchased from Thermo Fisher Scientific Inc. (Beijing, China). All other chemicals and reagents were analytical grade, unless otherwise statement.

2.2. Animals

BALB/C-nu/nu male nude mice (20 ± 2 g, eight-week-old) and Chinese white rabbits (2.0–2.3 kg) were purchased from the Shanghai Silaike Laboratory Animal Limited Liability Company. All the animals were pathogen free and allowed to access food and water freely. Animal experiments were carried out in accordance with the Guidelines for Animal Experimentation of China Pharmaceutical University (Nanjing, China) and protocol was approved by the Animal Ethics Committee of this institution.

2.3. Synthesis and characterization of anisamide-conjugated N-octyl-N-maleoyl-O-phosphoryl chitosan (a-OMPC)

2.3.1. Synthesis of N-octyl chitosan (OC)

N-octyl chitosan (OC) was synthesized through sequential procedure of "Schiff base-reduction" as reported previously (Qu et al., 2013). Briefly, 30 mL of methanol suspension of chitosan (1.5 g, 9 mmol) was stirred vigorously with octanal (9 mL, 55.5 mmol) at room temperature for 12 h. Next, $NaBH_4$ (570 mg, 15 mmol) was slowly added to the above mixture in three batches. After reaction for further 24 h, the suspension was filtrated, followed by washing the residue with water, water/methanol (1/1, v/v), methanol and diethyl ether, successively. Finally, 2.84 g crude product as a pale-yellow solid was obtained after drying at 60 °C under vacuum overnight.

2.3.2. Synthesis of N-octyl-N-maleoyl chitosan (OMC)

Four mL of *N, N*-dimethylformamide (DMF) suspension of OC (500 mg, 2.03 mmol) was stirred with maleic anhydride (200 mg, 2.04 mmol) at 90 °C for 6 h under nitrogen atmosphere. Afterward, the mixture was dropped into 14 mL of water under strongly mechanical agitation, followed by filtering and washing with 70 mL of water. Finally, 601 mg of OMC in a yield of 99.8% was gained after drying at 60 °C under vacuum overnight.

2.3.3. Synthesis of N-octyl-N-maleoyl-O-phosphoryl chitosan (OMPC)

PPA (950 mg) was carefully extruded into 5 mL of DMF suspension of OMC (500 mg, 1.69 mmol) in 5 min, followed by stirring at 70 °C. After reaction for 5 h, the DMF solution was poured in 25 mL of ice-cold water under mechanical agitation. The crude product was filtered, washed thrice with 100 mL of water and dissolved in 0.5% NaOH solution, successively. To remove the small molecular impurity, the above solution was loaded into a dialysis bag (molecular weight cut-off range (MWCO) of 10,000) for dialysis against distilled water. 600 mg of hydrophilic product in a yield of 71.4% as golden yellow powder was obtained after freeze drying. Besides, as the control of OMPC, *N*-octyl-*O*-phosphoryl chitosan (OPC) was synthesized using the similar method and introduced in Supporting information.

2.3.4. Synthesis of anisamide-conjugated OMPC (a-OMPC)

a-OMPC was synthesized *via* Michael addition between thiolated anisamide and double bond of maleoyl group of OMPC. Here, *N*-(*p*-anisoyl) cysteine as a thiolated anisamide was prepared through *N*-acylbenzotriazole and L-cysteine as reported previously (Fig. S1, Supporting information) (Katritzky et al., 2009). Briefly, equimolar *p*-anisoyl chloride and 1*H*-benzotriazole were stirred in tetrahydrofuran (THF) with slightly excessive triethylamine (TEA) at 20 °C for 2 h. Next, the obtained *N*-acylbenzotriazole (506 mg, 2 mmol) was added to the CH_3CN-H_2O (3/1, v/v) solution of L-cysteine (242 mg, 2 mmol) and TEA (202 mg, 2 mmol) and stirred at room temperature for 2 h. And then, the solvent was removed under reduced pressure, followed by washing with diluted hydrochloric acid and recrystallization in ethyl acetate/hexanes (3/1, v/v). Finally, 334 mg of *N*-(*p*-anisoyl) cysteine was in

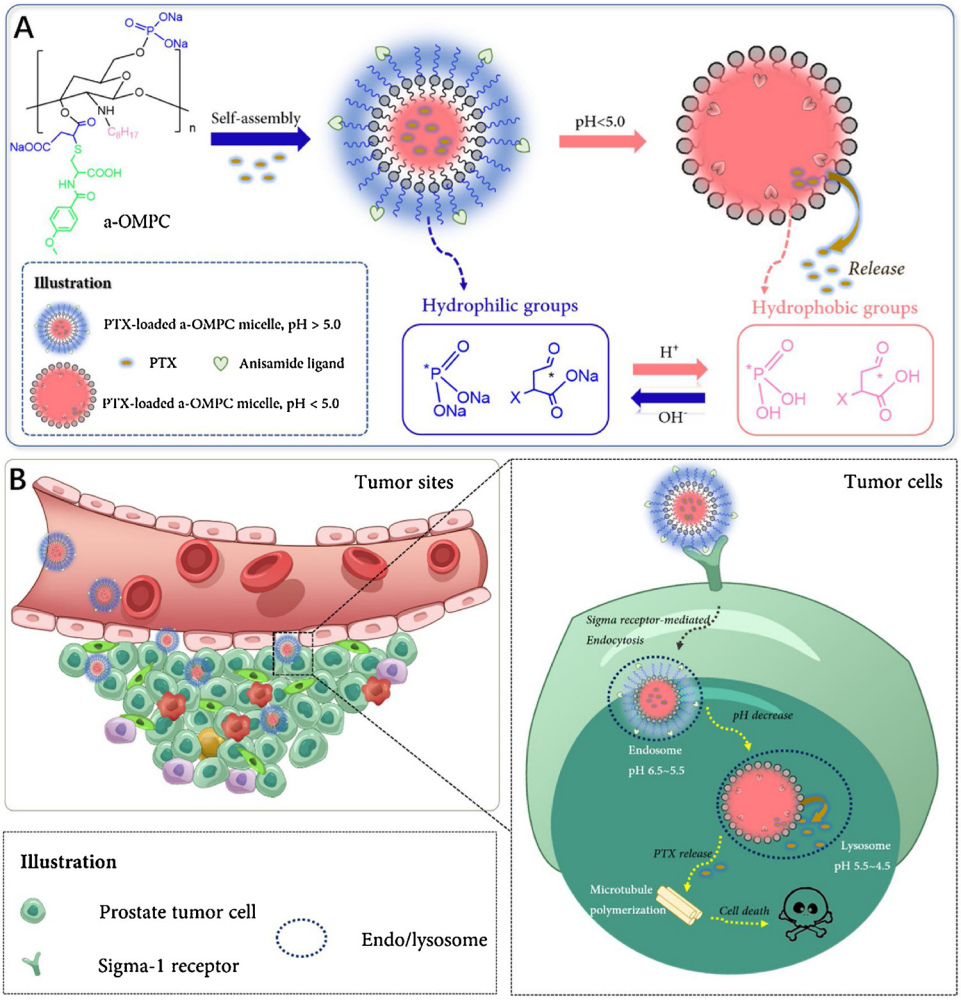

Scheme 1. Schematic representation for pH-responsive amphiphilic chitosan-based paclitaxel micelles for sigma-1 receptor targeted prostate cancer treatment. (A) a-OMPC can self-assemble into hydrophilic PTX-aM loading with PTX in neutral medium, while it can convert from hydrophilic to hydrophobic at pH lower than 5 because of pH-induced protonation of phosphate and maleate groups, followed by the drug release. (B) PTX-aM can accumulate at tumor site due to the enhanced permeation and retention (EPR) effect and then enter the PC-3 cell in a sigma-1 receptor-mediated pathway. After entrapping by endo/lysosomes, PTX-aM converts from hydrophilic to hydrophobic due to the acidic environment, leading to an unstable micellular structure and a rapid PTX release, which thus improves the antitumor efficacy.

yield of 62.1%.

N-(*p*-anisoyl) cysteine (510 mg, 2 mmol) and OMPC (510 mg) was stirred vigorously in 10 mL of 0.2% NaOH solution for 9 h at room temperature. Next, the reaction mixture was poured in 20 mL of ice-cold water under the mechanical agitation, followed by dialysis against distilled water for 24 h to remove the small molecular impurity. Finally, 608 mg of a-OMPC as pale-yellow powder was obtained after freeze drying in a total yield of 56.2% calculated with OC as a starting material.

The introduction of various groups into the backbone of chitosan was identified by Fourier transform infrared spectrometer (FT-IR, Nicolet 2000) with KBr pellets operating at room temperature (the number of scans, 32). The chemical structure of a-OMPC was confirmed by ^{1}H NMR using a Bruker AVANCE-300 spectrometer, the specific parameters is as follows, the number of scans is 16, the pulse is 10 μsec, the relaxation delay is 1 s, the spectral width is 19.9923 ppm/10000 Hz, and the transmitter frequency offset is 6.1175 ppm. The molecular weight of a-OMPC was measured by Gel permeation chromatography using dextran with different molecules as references. The degree of substituent (DS) of octyl and maleoyl group in a-OMPC was calculated through a Vario EL III elemental analyzer. The DS of anisamide in a-OMPC was quantified by the hydrogen integral ratio of benzene ring to chitosan backbone from ^{1}H NMR spectrum. For determination of DS of phosphoryl groups, the classic Fiske-Subbarow method was employed as reported previously (Durward & Harris, 1998). In addition, *N*-octyl-*O*-phosphoryl chitosan (OPC) without the modification of maleoyl groups was synthesized as control (Fig. S1). The DS of octyl and maleoyl groups of OMPC were calculated as the following equations (Qu et al., 2013):

$$DS\ of\ octyl\ groups = (C/N\ (\mathrm{mol})_{\mathrm{OC}} - C/N\ (\mathrm{mol})_{\mathrm{chitosan}})/8;$$

$$DS\ of\ maleoyl\ groups = (C/N\ (\mathrm{mol})_{\mathrm{OMC}} - C/N\ (\mathrm{mol})_{\mathrm{OC}})/4.$$

2.4. Critical micelle concentration (CMC) determination

The critical micelle concentration (CMC) of a-OMPC was determined by fluorescence spectroscopy using pyrene as a probe (Li et al., 2017). 100 μL of acetone solution containing 3×10^{-5} M of pyrene were prepared, followed by evaporation of organic solvent at room temperature overnight. After mixing with the above pyrene, 5 mL of aqueous solution of a-OMPC (concentration ranged from 1×10^{-4} to 1 mg/mL) was sonicated for 30 min and incubated at 65 °C for 3 h, successively. Next, each of sample was filtrated with 0.22 μm pore-sized microfiltration membrane when the mixture cooled to room temperature. The excitation spectra (300–360 nm) of the solutions were recorded at an emission wavelength of 390 nm, with the excitation and emission bandwidths as 3 nm. The ratios of the fluorescence intensity at 337 nm to 334 nm (I_{337}/I_{334}) were recorded to plot curve using the a-OMPC concentration as abscissa. The CMC value was determined according to the intersection point of two tangents along the curve. Likewise, the CMC value of OMPC was determined by the similar method.

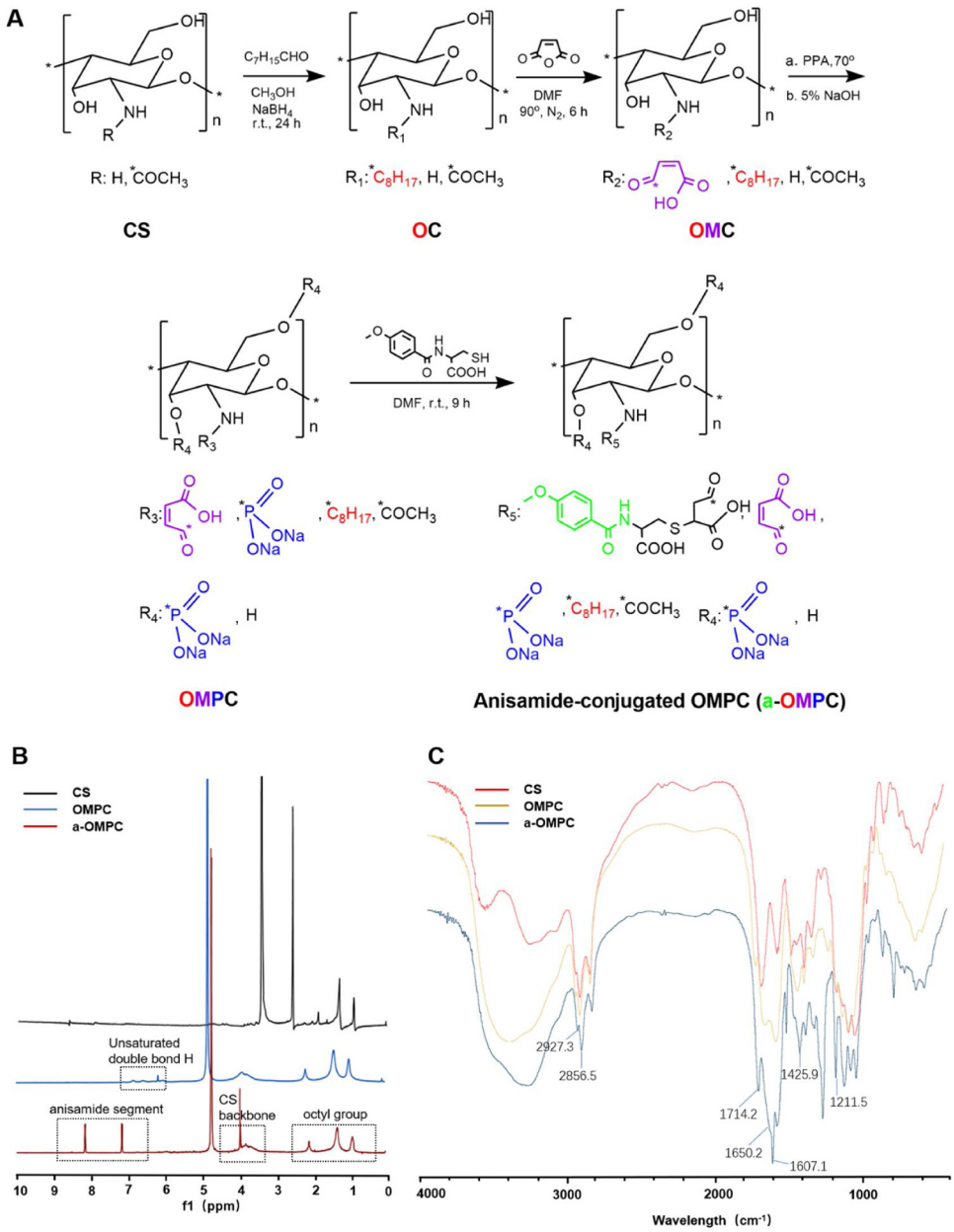

Fig. 1. Synthesis and characterization. (A) Synthetic route of a-OMPC. (B) ^{1}H NMR spectrum of chitosan derivatives. (C) FT-IR spectrum of chitosan derivatives.

Table 1
DS of each group of various chitosan derivatives.

Compound	octyl	maleoyl	phosphoryl	anisamide
OC	0.60	N/A	N/A	N/A
OMC	0.60	0.40	N/A	N/A
OPC	0.60	NA	1.64	NA
OMPC	0.60	0.40	1.07	N/A
a-OMPC	0.60	0.40	1.07	0.40

2.5. Preparation and characterization of PTX-aM

0.2 mL of PTX ethanol solution was rapidly dropped into 2.5 mL of a-OMPC aqueous solution under vigorously magnetic stirring at room temperature, with the mass ratio of PTX to a-OMPC as 1/1. After stirring for 5 min, the mixture was immediately dialyzed against distilled water for 12 h using dialysis membrane (10,000 MW cutoff) to obtain PTX-aM (Mo et al., 2011; Qu et al., 2013; Zhang et al., 2016). Likewise, PTX-loaded OMPC micelles (PTX-M) was prepared using the similar method, except that a-OMPC was replaced with OMPC. DiO-labelled PTX-aM (DiO/PTX-aM), DiI-labelled PTX-aM (DiI/PTX-aM) and DiD-labelled PTX-aM (DiD/PTX-aM) were synthesized through co-loading of PTX and corresponding dyes at the mass ratio of 500/2 (w/w). To measure drug encapsulation efficiency (DEE) and drug loading efficiency (DLE), the micellar solution was filtered with a 0.22 μm pore-sized microfiltration membrane, freeze-dried through lyophilizer and quantified PTX concentration by HPLC, successively. The DEE and DLE of micelles were calculated by the following equations: DEE (%) = $W_1/W_A \times 100\%$; DLE (%) = $W_2/W_B \times 100\%$, where W_1, W_2, W_A and W_B represent the weight of encapsulated PTX in micellar solution, the weight of contained PTX in freeze-dried micelles, the weight of feeding PTX and the weight of freeze-dried micelles, respectively.

The size and zeta potential of micelles was measured by a Zeta potential analyzer (Zeta Plus, Brookhaven, USA). The morphology of micelles was investigated by transmission electron microscope (TEM, JEM-200CX, JEOL Ltd., Japan) using 1% (v%) phosphomolybdic acid as

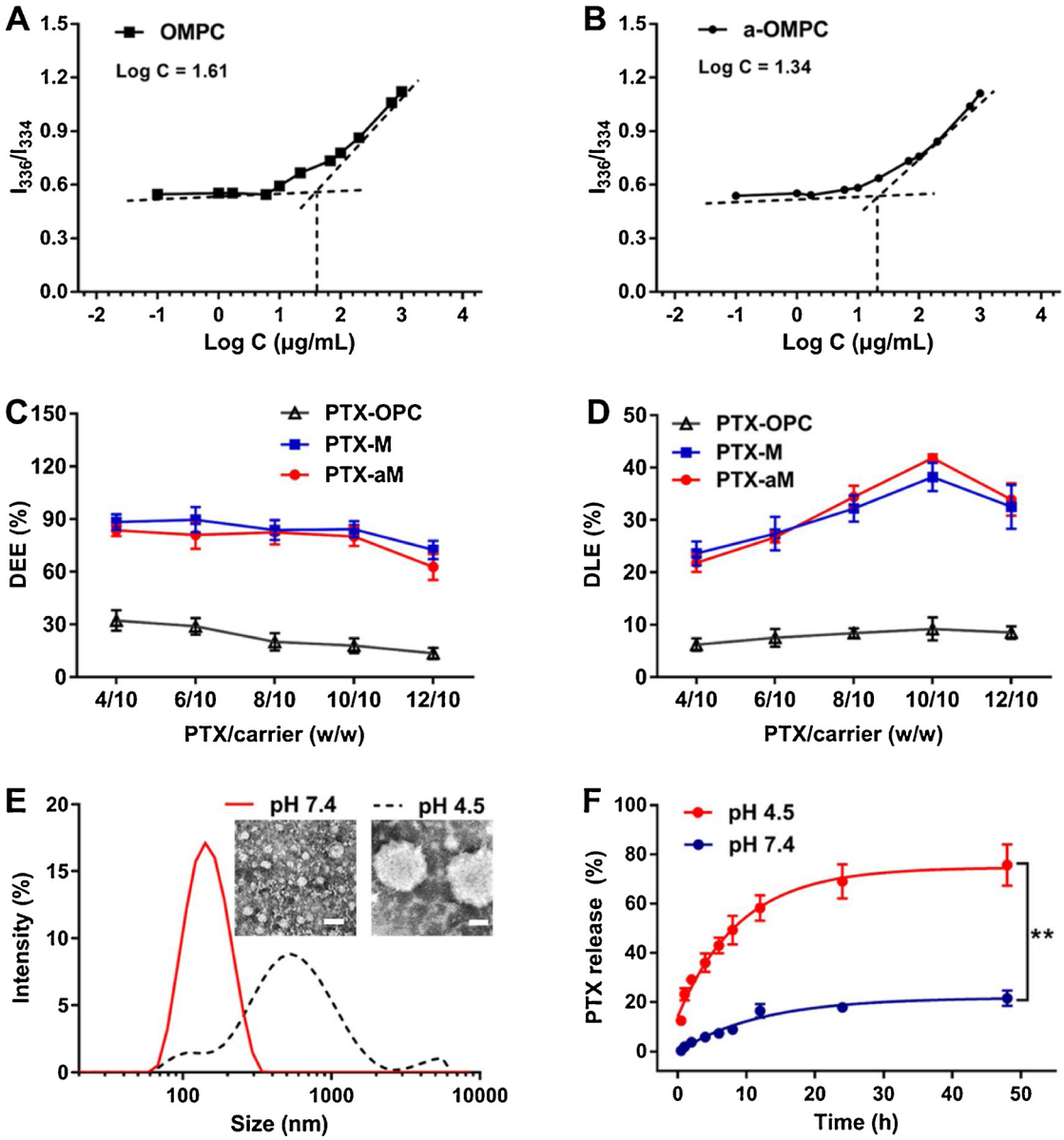

Fig. 2. Characterization of micelles. (A–B) Determination of CMC of OMPC and a-OMPC. (C) Drug encapsulation efficiency (DEE) of various micelles at different mass ratios of PTX to carriers. (D) Drug loading efficiency (DLE) of various micelles at different mass ratios of PTX to carriers. (E) Size distribution of a-OMPC micelles at different pH values. Inset: TEM images of PTX-aM at pH 7.4 and 4.5. The scale bar is 200 nm. (F) Accumulative PTX release profile of PTX-aM under different pH environments (n = 3). $^{**}P < 0.01$; Data represented as mean ± SD.

Table 2
Characterizations of various PTX-loaded micelles (n = 3, $^{*}P < 0.05$ *vs* PTX-M).

Formulation	Size (nm)	PDI	Zeta (mv)
PTX-M	132.6 ± 4.3	0.118 ± 0.002	−22.85 ± 1.42
PTX-aM	162.8 ± 3.2*	0.137 ± 0.008	−29.69 ± 1.22*

staining agent.

2.6. In vitro drug release

1 ml of PTX-aM containing 1 mg of PTX were added into a dialysis bag, followed by immersion in 100 mL of release medium at 37 °C with stirring at 60 rpm. The release medium included PB of pH 7.4 and acetate buffer of pH 4.5 with 0.1% (w/v) Tween 80 in accordance with a sink condition. At predetermined time intervals (0.5–48 h), 1 mL of release medium was withdrawn, followed by replacing corresponding equivalent fresh release medium and filtration through a 0.22 μm pore-sized polycarbonate membrane filter. The accumulative release of PTX was calculated after quantifying by HPLC.

2.7. Cells culture

Human prostate tumor cells (PC-3) and murine prostate tumor cells (RM-1) were purchased from the cell bank of Chinese Academy of Sciences. Two types of prostate tumor cells were cultured in Ham's F-12 with 12% (v/v) FBS. Culture medium were added 100 U/mL penicillin and 100 μg/mL streptomycin. The cells were cultured in an incubator at 37 °C under an atmosphere of 5% CO_2 and 90% relative humidity, respectively.

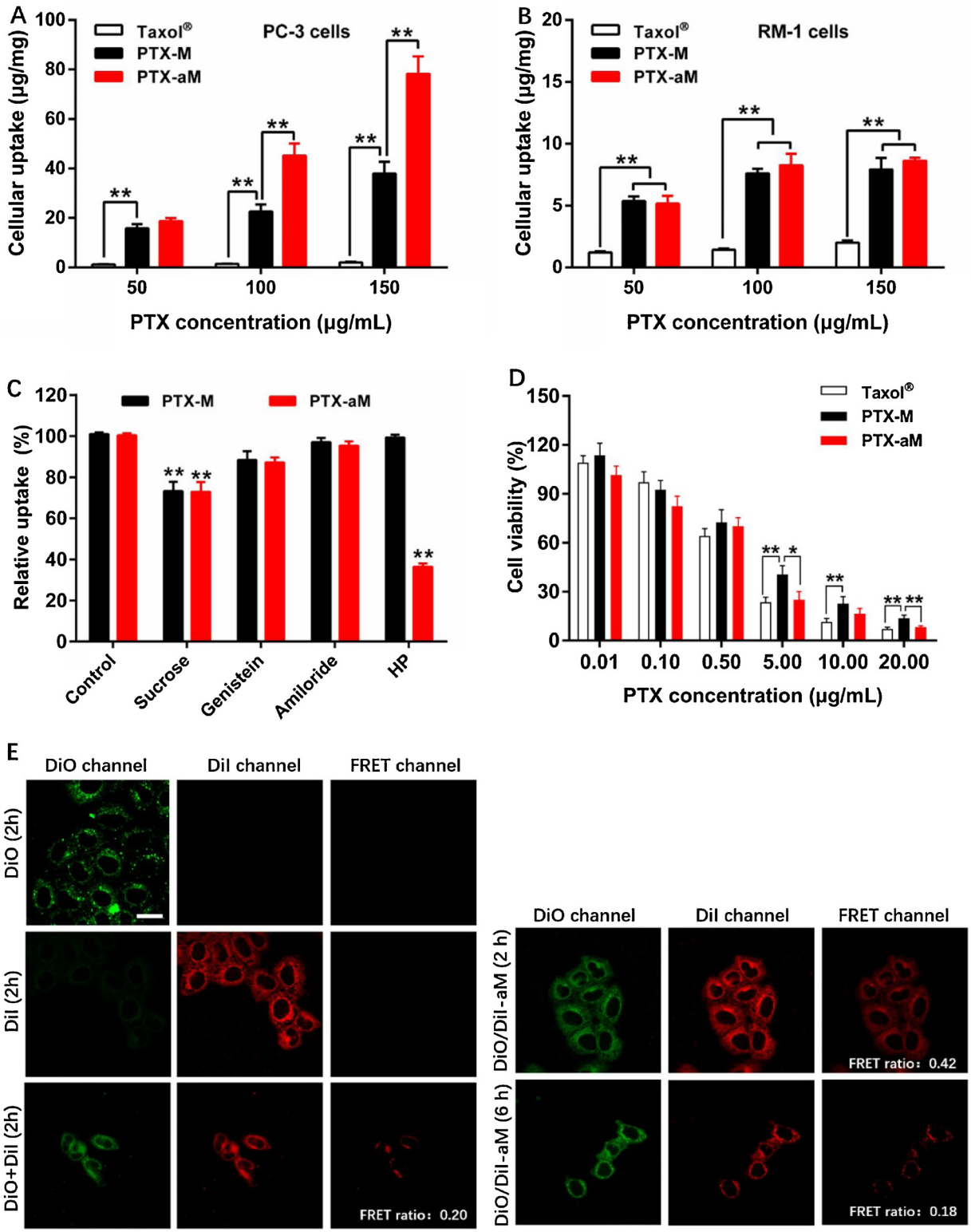

Fig. 3. Cellular studies. Cellular uptake of various formulations on (A) PC-3 and (B) RM-1 cells (n = 4). $^{**}P < 0.01$; Data represented as mean ± SD. (C) Mechanism of cellular uptake of micelles (n = 4). $^{**}P < 0.01$; Data represented as mean ± SD. (D) Antiproliferative effect of various PTX formulations against PC-3 cells (n = 6). $^{*}P < 0.05$, $^{**}P < 0.01$; Data represented as mean ± SD. (E) Intracellular FRET effect after treatment with DiI/DiO-aM. Bar scale is 20 μm.

2.8. Cellular studies

2.8.1. Cellular uptake of PTX

Ten thousand of PC-3/RM-1 cells were seeded into 24-well plates until the confluence reached 80%. 400 μL of PTX-aM solutions with PTX concentration of 50, 100 and 150 μg/mL were treated with cancer cells at 37 °C for 2 h. Thereafter, the cells were rinsed with ice-cold PBS thrice, followed by incubation with 200 μL of 0.1% SDS cell lysis buffer for 3 min. The intracellular PTX were quantified by HPLC and the cell protein was measured by classic BCA protein assay kit. Cellular uptake of PTX on cancer cells was calculated as the following equation: cellular uptake (μg PTX/mg protein) = $A_{intracellular\ PTX}/A_{cell\ protein}$, where

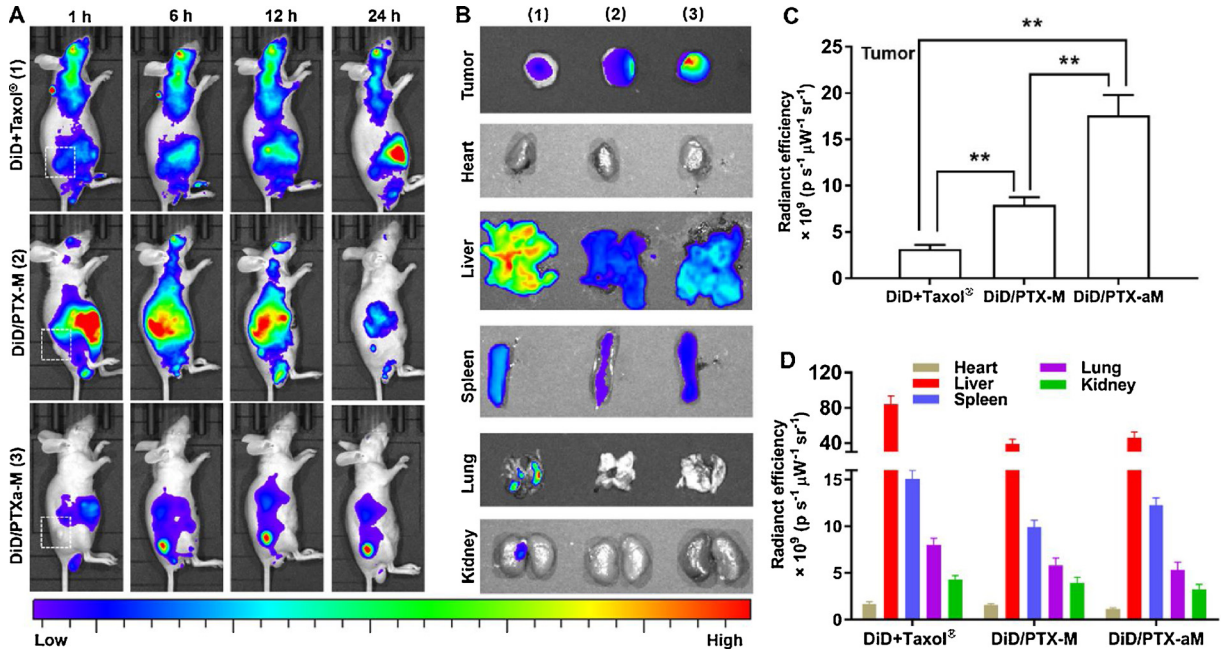

Fig. 4. Investigation of biodistribution. (A) In vivo image of mice treated with different DiD-labelled formulations. (B) Ex vivo image of organs of mice after 24 h of treatment. (C) Fluorescence intensity of harvested tumors of mice treated with DiD-labelled formulations (n = 3). $^{**}P < 0.01$; Data represented as mean ± SD. (D) Fluorescence intensity of harvested normal organs of mice treated with DiD-labelled formulations (n = 3). $^{**}P < 0.01$; Data represented as mean ± SD.

$A_{intracellular\ PTX}$ and $A_{cell\ protein}$ represent the amount of intracellular PTX and cellular protein, respectively. Accordingly, the cellular uptake of PTX-M and Taxol® were studied as the similar method.

2.8.2. Endocytosis pathways

Ten thousand of PC-3/RM-1 cells were seeded into 24-well plates until the confluence reached 80%. Prior to experiment, the cancer cells were pretreated with various chemical internalization inhibitors for 30 min as follows, (1) inhibitor of sigma receptor-mediated endocytosis: 19 μg/mL of haloperidol (HP); (2) inhibitor of clathrin-mediated endocytosis: 154 mg/mL of sucrose; (3) inhibitor of caveolae-mediated endocytosis: 54 μg/mL of genistein; (4) inhibitor of micropinocytosis: 133 μg/mL of amiloride (Dreifuss et al., 2018). At the end of the incubation, the cells were further treated with PTX-M and PTX-aM in the presence of the corresponding inhibitor for 2 h, respectively. Finally, the cellular uptake of PTX was determined as the above-mentioned method. The relative cellular uptake ratio was calculated as the following formulations: uptake ratio (%) = cellular uptake of sample/cellular uptake of control × 100%.

2.8.3. Intracellular delivery

In order to trace the intracellular delivery of micelles after crossing over the cell membrane, PTX-aM was labelled with green fluorescence (FITC/PTX-aM) through conjugation of FITC onto the residual amino group of a-OMPC. 1×10^6 of PC-3 cells were seeded on a polylysine-coated slide at 37 °C. After reaching 60% confluence, the cells were co-incubated with FITC/PTX-aM at a FITC concentration of 15 μM for 4 h. Afterward, the cells were rinsed by 4 °C PBS thrice, followed by staining with 100 nM LysoTracker Red (Invitrogen, USA) for 30 min at 37 °C and fixing with 4% paraformaldehyde for 30 min (Guo et al., 2014). Finally, the cells were adequately washed with PBS and immediately observed by confocal laser scanning microscopy (CLSM, Olympus, Japan).

2.8.4. Antiproliferative effect

Five thousand of PC-3 cells were seeded into 96-well plates and cultured overnight. After removal of culture medium, the cells were respectively treated with PTX-M and PTX-aM solution at the PTX concentrations ranging from 0.1 to 20 μg/mL, and Taxol® was used as a positive control group. After 24 h of incubation, the cells were stained with the PBS solution of MTT (5 mg/mL) for further 4 h at room temperature. At the end of this time, the resultant medium was replaced with 200 μL of DMSO. The absorbance was measured using a microplate reader at 492 nm (Varioskan Flash, Thermo Fisher Scientific, USA).

2.8.5. Intracellular stability of micelles

In this part, the fluorescence resonance energy transfer (FRET) technology was used to explore the potential intracellular stability of micelles (Breunig, Lungwitz, Liebl, & Goepferich, 2006). DiO and DiI, as a pair of FRET, were used to visualize PTX-aM. Briefly, 1×10^6 of PC-3 cells were cultured on a polylysine-coated slide until reaching 60% confluence, and then co-incubated with DiO, DiI, DiO + DiI and DiO/DiI/PTX-aM at a DiO or/and DiI concentration of 2 μM for 4 h, respectively. Afterward, the cells were rinsed by 4 °C PBS thrice, followed by fixing with 4% paraformaldehyde for 30 min at room temperature. After washing with PBS, the samples were immediately observed by CLSM (Olympus, Japan) at DiO channel (Ex:488 nm, Em 501 nm), DiO channel (Ex:545 nm, Em 565 nm) and FRET channel (Ex:488 nm, Em 565 nm), respectively.

2.9. PC-3 tumor-bearing xenograft model

Twenty-four male nude mice (20 ± 2 g) were randomly divided into four groups according to the body weight. 0.2 mL of suspension containing 2×10^7 PC-3 cells was subcutaneously injected to the armpit of right anterior limb of each mouse. When the tumor volume reached 80–100 mm^3, the mice was used in the following studies.

2.10. In vivo image

PC-3 tumor-bearing xenograft nude mice were intravenously administrated with DiD + Taxol®, DiD/PTX-M and DiD/PTX-aM at a DiD dose of 50 nmol/kg. Each of isoflurane-anaesthetized mice were observed under in vivo imaging system (IVIS Lumina II) at predetermined time intervals post-injection. The excitation and emission were set at 645 nm and 665 nm, respectively. At 24 h post-treatment, mice were sacrificed. The tumor and main normal organs were collected and

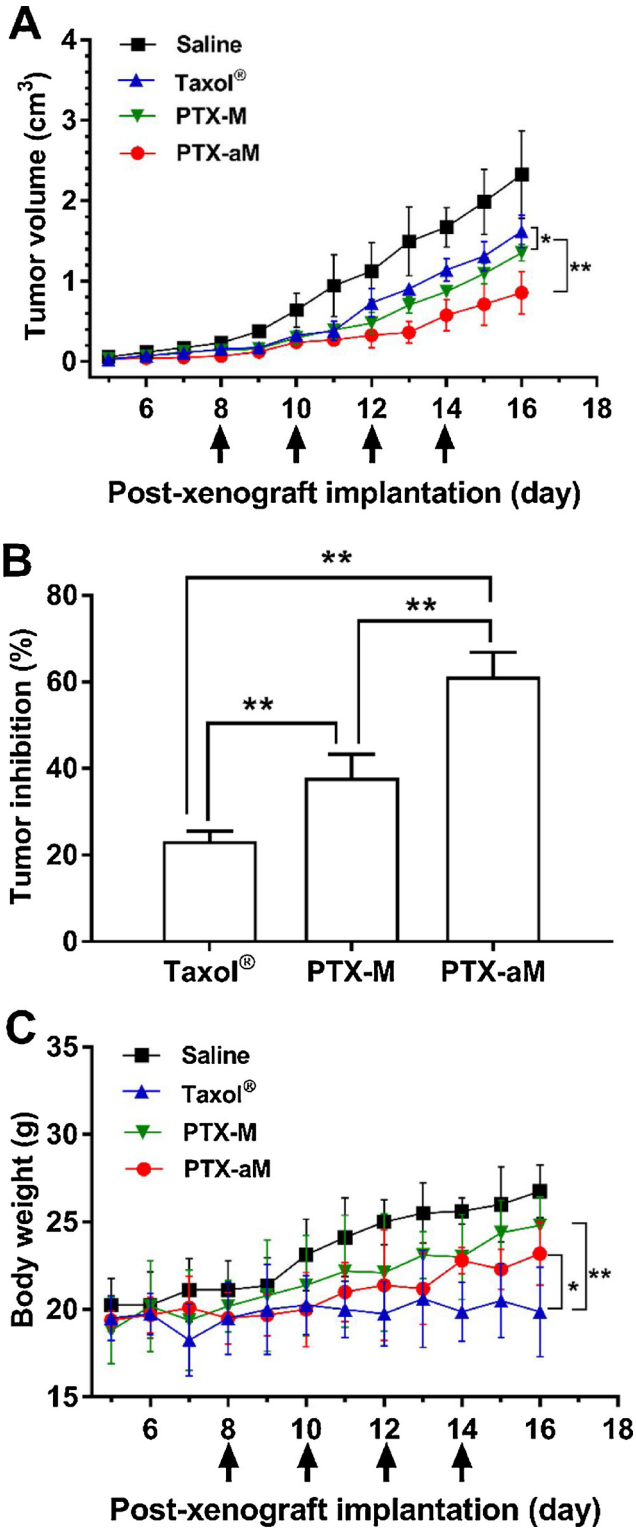

Fig. 5. In vivo anticancer efficacy. (A) Tumor growth of PC-3 tumor-bearing mice after intravenous injection of different PTX formulations (n = 6). $^{*}P < 0.05$, $^{**}P < 0.01$; Data represented as mean ± SD. (B) Tumor inhibition rate of PC-3 tumor-bearing mice after intravenous injection of different PTX formulations (n = 6). $^{**}P < 0.01$; Data represented as mean ± SD. (C) Changes in body weight of PC-3 tumor-bearing mice during and after the treatment (n = 6). $^{*}P < 0.05$, $^{**}P < 0.01$; Data represented as mean ± SD.

observed by the imaging system (IVIS Lumina II). Region-of-interests (ROI) tool was used to quantified the fluorescence intensity (Zhou et al., 2018).

2.11. Antitumor efficacy

Mice were randomly divided into four groups (n = 6) according to the tumor size, and then intravenously injected with saline, Taxol®, PTX-M and PTX-aM at a PTX dose of 10 mg/kg once every two days. The length and width of tumor was measured by vernier calipers during the treatment. The tumor volume was calculated according to the following formula: tumor volume (mm^3) = 0.5 × length × $width^2$. Body weight and survival time of mice were recorded during the treatment.

2.12. Hemolytic assay

In this part, we investigated the potential hemolysis of OMPC in vivo using pure water and saline as positive and negative control, respectively. 10 mL of Rabbit blood was collected from the auricular vein of rabbit, followed by removing the azelon through gentle rotation with cotton swabs. Rabbit red blood cells (RBCs) were separated by refrigeration centrifuge at 3000 rpm ×10 min, followed by washing adequately with sterile PBS. After 50-fold dilution, the obtained RBCs were mixed with different concentrations of OMPC, saline and pure water. After incubation at 37 °C for 4 h, the absorbance of each sample was measured by microplate reader at 540 nm, and the relative hemolytic rate was calculated as the following equation, relative hemolysis (%) = (absorbance of sample - absorbance of pure water)/(absorbance of saline - absorbance of pure water) × 100% (Li et al., 2018).

2.13. Acute toxic assay

To explore the potential acute toxicity *in vivo*, the mice were single-treated with high dose of OMPC. Prior to experiment, 50 mice were randomly divided into 5 groups according to the body weight. 0.2 mL of OMPC solution was intravenously administrated at dose ranged from 300 mg/kg to 122 mg/kg. The survival was recorded during the following 14 days. Chitosan with the same dose was used as control group.

2.14. Statistical analysis

Data are given as mean ± S.D. Statistical significance was tested by two-tailed Student's *t*-test or one-way ANOVA. Statistical significance was set at $^{*}P < 0.05$, and extremely significance was set at $^{**}P < 0.01$.

3. Results and discussion

3.1. Synthesis and characterization of amphiphilic chitosan

As shown in Fig. 1A, a-OMPC was synthesized through *N*-octylation, *N*,*O*-maleoylation, *O*-phosphorylation, and conjugation of sulfhydryl anisamide onto double bond of maleoyl groups through Michael addition, successively. Octyl and phosphoryl groups act as hydrophobic and hydrophilic segments, respectively. A certain amount of maleoyl group provides suited chemical sites for sulfhydryl anisamide. Fig. 1B showed the ^{1}H-NMR spectrums of various compounds. Three intensive signals of OMPC in D_2O at δ (ppm) 0.87, 1.25 and 2.12 were attributed to H of octyl groups. One broad peak belonging to chitosan backbone appeared from δ (ppm) 3.41 to 4.43 (Qu et al., 2013). Besides, we found four weak spilt peaks of double bonds at δ (ppm) 6.05, 6.21, 6.50 and 6.81, verifying the conjugation of maleoyl groups with 2-NH_2 and 6-OH of chitosan (Almeida et al., 2014). Of note, two new signals of a-OMPC appeared at δ (ppm) 7.16, 8.18, probably attributed to the aromatic ring of anisamide segment (Katritzky et al., 2009). As expected, the above-mentioned characteristic signals of double bond belonging to maleoyl groups disappeared, validating the conjugation of thiolated anisamide with OMPC. As the FT-IR characterization depicted in Fig. 1C, characteristic peaks at 3563.6 and 1564.2 cm^{-1} were observed from the FT-IR spectrum of chitosan, which could be attributed to the

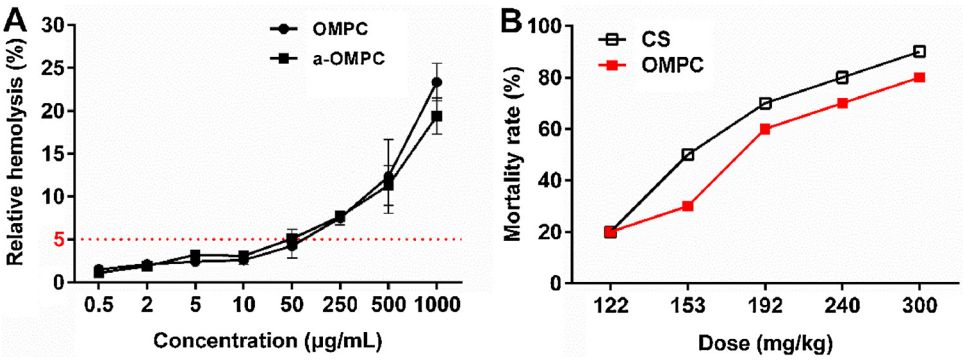

Fig. 6. Toxicity of chitosan derivative. (A) Relative hemolysis of rabbit RBCs after incubation with OMPC and a-OMPC at concentrations ranged from 0.5 to 1000 μg/mL (n = 6); Data represented as mean ± SD. (B) Observation of mortality rate of mice administrated with CS and OMPC at doses ranged from 122 to 300 mg/kg (n = 10); Data represented as mean ± SD.

stretching and bending vibration of 2-NH_2, respectively. The appearance of new peaks at 2927.3, 2856.5 and 1381.6 cm^{-1} the weakened NH_2 signal suggests the conjugation of octyl groups with amino segments of chitosan. In addition, the appearance of new peaks at 1598.1 and 1650.2 cm^{-1} might belong to double bond and amide after introduction of maleoyl groups (Almeida et al., 2014). Notably, the new signal at 1211.5 cm^{-1} representing stretching vibration of P═O indicated the incorporation of phosphoryl groups into 6-OH and/or 3-OH groups of chitosan (Qu et al., 2019; Zhang et al., 2016). As for characterization of a-OMPC, the observation of two specific peaks at 1607.1 and 1513.0 cm^{-1} (vibration of benzene ring) and the disappearance of above-mentioned double bond signal indicates that anisamide segment was successfully linked with OMPC. The molecular weight of a-OMPC ranged from 80 kDa to 400 kDa studied by GPC (see Fig. S2), suggesting substantial groups were successfully conjugated with active sites of chitosan.

As shown in Table 1, the DS of octyl and maleoyl groups in OMPC were approximately 60% and 40% respectively, through calculating the molar ratio of C to N using element analysis. The DS of phosphoryl groups of OMPC was measured to be 107% using classic Fiske-Subbarow method (Durward & Harris, 1998), suggesting that 3-OH and 6-OH were both phosphorylated. The DS of anisamide was around 40% through calculating the integral ratio of H signal at 7.52 ppm to 4.43 ppm, indicating that the double bond of maleoyl groups was almost totally occupied by thiolated anisamide.

As our hypothesis, simultaneous introduction of maleoyl and phosphoryl group brings chitosan flexible solubility in both water and organic system, which is of great importance to pH-responsive release. To proof our idea, the solubility of various chitosan derivatives was tested in different solvents. As list in Table S1, OMC was readily capable of dissolving in DMSO, DMF and ethanol (> 500 mg/mL). OPC, as a control of OMPC, was soluble in water (> 100 mg/mL), but precipitated rapidly as pH decreased up to 4.5. In contrast, OMPC can dissolve in water at pH 7.4 and in organic solvent at pH 4.5, showing a pH-dependent flexibility in solubility.

3.2. CMC determination

To evaluate the potential *in vivo* stability of micelles, CMC of chitosan derivatives was measured by fluorescence spectroscopy in the presence of pyrene. Generally, CMC was the threshold concentration, where the intensity ratio I337/I334 became increase sharply (Li et al., 2017). As shown in Fig. 2A and B, CMC values of OMPC and a-OMPC were respectively 40.7 μg/mL and 18.4 μg/mL at pH 7.4. However, the CMC of two chitosan derivatives obviously dropped with pH value decreased, and even undetectable at pH 4.5 (Table S2), probably due to the protonation of maleoyl and phosphoryl groups and consequent imbalance in hydrophilic and hydrophobic groups.

3.3. Characterizations of micelles

PTX-aM was prepared by "injection-dialysis" method as reported previously (Qu et al., 2013). Using the same method, we also prepared PTX-loaded OMPC micelles (PTX-M) without targeting ability and PTX-loaded OPC micelles (PTX-OPC) as controls. Different feeding ratio of PTX to carrier determined DEE and DLE. As shown in Fig. 2C and D, PTX-aM displayed the optimal DEE and DLE with a mass ratio of 10/10 (PTX/a-OMPC). By comparison, the DLE and DEE of PTX-OPC was remarkably lower than that of PTX-M and PTX-aM, further suggesting the significance of maleoyl units in payloads loading. And we would not consider PTX-OPC as drug vector due to the low drug capacity.

As listed in Table 2, the particle size of PTX-aM was 162.8 ± 3.2 nm, which was significantly larger than that of PTX-M, probably because the water solubility of a-OMPC was influenced after conjugation with hydrophobic anisamide. The zeta potential of PTX-aM was −29.69 ± 1.22 mV and decreased significantly compared with that of PTX-M, which was associated with more introduction of carboxylate group. Of note, the average size of PTX-aM dramatically increased up to 500 nm with a broad PDI with the pH decreased to 4.5 (Fig. 2E), suggesting that the micelle's inner core swelled sharply as a rapid consumption of the outer hydrophilic layer. Such pH-triggered size conversion probably decreased the water-solubility of vectors, destroyed the stability of micelles and accelerated the following drug release. This result was further confirmed by the accumulative PTX release of PTX-aM at two different pH values (Fig. 2F). At pH 7.4, 21.58% of PTX was released from PTX-aM within 48 h, while PTX was released significantly faster as the pH decreased.

3.4. Cellular uptake and intracellular delivery

To evaluate the affinity of PTX-aM to sigma-1 receptor overexpressed prostate cancer cells, PC-3 cells overexpressed sigma-1 receptor were used for investigation, and RM-1 cells negatively expressed sigma receptor were taken as control (Zhang & Russell, 2006). As shown in Fig. 3A, the cellular uptake of two PTX-loaded micelles was greatly improved compared with that of Taxol® (**$P < 0.01$), showing an inherent superiority of polymeric micelles in internalization. Notably, PTX intracellular accumulation of cells treated with PTX-aM were significantly higher than PTX-M (**$P < 0.01$) at the medium and high dose, suggesting that anisamide functionalization was capable of enhancing the cellular uptake *via* sigma-1 receptor-mediated endocytosis. In contrast, there was no significant difference in internalization between PTX-M and PTX-aM on RM-1 cells (Fig. 3B), validating an advantage of anisamide modification on sigma receptor-overexpressed cells.

To further figure out the mechanism of cellular uptake, we observed the alternation in endocytosis after pretreatment with specific internalization inhibitors. As exhibited in Fig. 3C, PC-3 cellular uptake of PTX-aM was significantly suppressed after pretreatment with 19 μg/mL of haloperidol (HP), a compound with high affinity for sigma receptor

(Maurice & Su, 2009; Olivieri et al., 2016) (**$P < 0.01$), which had no impact on cellular uptake of PTX-M. It suggested that the enhancement on uptake of PTX-aM was highly correlated with sigma-1 receptor. In addition, pretreatment with sucrose, an inhibitor for clathrin-mediated endocytosis, led to obvious decrease in cellular uptake of two PTX-loaded micelles (*$P < 0.01$), implying that particles probably distributed in endo/lysosomes after crossing over cell membrane. It was further evidenced by the confocal image of PC3 cells after incubation with FITC/PTX-aM for 4 h. We found the obvious overlap of FITC (green) and endo/lysosomes (red) within cells (Fig. S3), indicating the drug delivery system probably accumulated in lysosomes (pH 4.5–5.5) where the acidic environment could switch on the valve of drug release. As our hypothesis, the rapid drug release of PTX-aM in endo/lysosomes might be favorable for killing tumor cells.

3.5. In vitro anticancer effect

The antiproliferative effect of PTX formulations against PC-3 cells was evaluated using the MTT assay. As shown in Fig. 3D, Taxol® displayed a strong antiproliferative effect at a PTX concentration of 0.5 μg/mL. After micellular assembly, the growth inhibition of PTX-M against PC-3 cells was obviously observed only when PTX concentration reached 5 μg/mL, that is probably associated with slow release and non-optimal cellular uptake. As expected, PTX-aM displayed a significant enhancement on cytotoxicity compared with PTX-M (*$P < 0.05$, **$P < 0.01$), implying that anisamide-mediated internalization and rapid drug release could promote the in vitro anticancer effect in sigma-1 receptor-overexpressed cell lines.

3.6. Intracellular FRET effect

As our hypothesis, PTX-aM was capable of releasing PTX rapidly in the endo/lysosomal environment due to the low water solubility of vehicle. However, we have not known the potential changes of the structure integrity of PTX-aM during the protonation process yet. Here, we employed the FRET technology to explore the intracellular stability through co-labelling micelles with DiO and DiI (a FRET pair). As shown in Fig. 3E, the cells treated with DiO + DiI occurred hardly FRET phenomenon. However, we found relatively obvious signal on FRET channel in DiO/DiI-aM-treated group after 2 h of incubation, indicating that two dyes were mainly distributed within a small core of the micelle (Abraham, Santala, Tkachenko, & Karp, 2014; Zamaleeva et al., 2015). According to the previous equation (Qu et al., 2018), the FRET ratio of DiO/DiI-aM-treated cells was 2.1 times of that of DiO + DiI groups. As expected, the FRET ratio of cells treated with DiO/DiI-aM sharply decreased with the incubation time expended as 6 h. These results suggested that the hydrophobic core of the micelle was compact at initial stage of internalization. With further acidification, the micelle's hydrophobic core became swell increasingly, leading to two dyes separated each other and even potentially leaked from the particle.

3.7. In vivo tumor targeting

To visualize the tumor-specific accumulation, PC-3 tumor xenograft-bearing nude mice were administrated with DiD-labelled micelles, and DiD + Taxol® was taken as a control. As shown in Fig. 4A, mice treated with DiD + Taxol® showed a non-selective biodistribution in the period of the observation. Due to the recognition by the reticuloendothelial system (RES), the intensive fluorescence of DiD/PTX-M was found in the whole abdomen and spine during 12 h post injection. The area of tumor also appeared fluorescence signal from 6 to 24 h. As expected, DiD/PTX-aM displayed the obviously stronger tumor-targeted ability compared with DiD/PTX-M during the whole period of the observation, suggesting the significance of anisamide-modification for sigma-1 receptor targeting. The fluorescence of ex vivo tumors and normal organs was acquired at 24 h post injection. As shown in Fig. 4B, the tumor of DiD/PTX-aM-treated mice exhibited the overwhelming fluorescence, that was 6.1-fold and 2.2-fold of that of DiD + Taxol® (**$P < 0.01$) and DiD/PTX-M-treated mice (**$P < 0.01$), respectively (Fig. 4C). It indicated that micelle conjugated with anisamide ligand was favorable to affiliate to sigma-1 receptor-overexpressed tumor tissues. As for the normal organs, treatment of DiD + Taxol® led to the obviously higher accumulation at lung, liver and spleen than that of DiD/PTX-M and DiD/PTX-aM (Fig. 4D), further validating the non-selective distribution of free drug. Although the fluorescence distribution at liver and spleen was still detectable, the undesired accumulation mitigated obviously after treatment with micelles.

3.8. In vivo antitumor efficacy

For proof of our idea, PTX-aM was employed to treat PC-3 tumor xenograft nude mice, and Taxol® and PTX-M were taken as controls. As shown in Fig. 5A, all PTX foumalutions significantly inhibited the tumor growth compared with saline. The tumor volumes of mice treated with PTX-M at day 16 was obviously smaller than that of Taxol® group (*$P < 0.05$), which was attributed to EPR-associated passive tumor targeting and pH-responsive drug release. Notably, PTX-aM exhibited an evidently stronger inhibition of tumor growth relative to PTX-M (**$P < 0.01$), validating an advantage of anisamide-modification in tumor-targeted drug delivery. As shown in Fig. 5B, the inhibition rate of tumor growth after PTX-aM treatment was approximately 60%, which was markedly higher than PTX-M and Taxol® (**$P < 0.05$), further proving the rationality of sigma-1 receptor targeting and pH-responsive release. In addition to anticancer activity, PTX-aM did not show obvious weight loss which was found in Taxol® treatment (Fig. 5C), indicating that PTX-loaded micelles are capable of attenuating the systemic toxicity through decreasing in vivo off-targeting. Most importantly, two PTX-loaded micelles exhibited the most distinguished effect on extending the survival period of PC-3 tumor-bearing nude mice (Fig. S4). Overall, PTX-aM can significantly suppress the tumor growth, notably prolong the survival time and reduce side effects in vivo.

3.9. Hemolysis and acute toxicity

For injectable anticancer polymeric micelle, the safety of vehicle is another cruical factor in clinic application in addition to encapsulated chemotherapeutic agents. In this part, we investigated the potential hemolysis in blood and lethal median dose (LD50) to evaluate the systemic toxicity of chitosan derivative. As shown in Fig. 6A, the relative hemolysis of RBC was below 10% even incubation with 250 μg/mL of OMPC and a-OMPC. It indicated that PTX-loaded chitosan micelles had low risk of hemolysis during intravenous injection (Chiou, 1974). In addition, Fig. 6B and Table S3 exhibited the mortality rate of mice after administration with excessive OMPC solution in a short period of time. 60% of mice died after treatment with 192 mg/kg OMPC in 14 days. In contrast, equivalent dose of chitosan solution resulted in 100% mortality. The LD50 and 95% confidence interval of OMPC and chitosan were 186.94 (168.65–207.21) mg/kg and 104.23 (95.23–115.62) mg/kg, respectively. It suggested that OMPC with various modifications greatly reduced the potential toxicity than chitosan.

4. Conclusion

In summary, the amphiphilic a-OMPC containing octyl, maleoyl, phosphoryl and anisamide segments was synthesized and confirmed by multidimensional characterizations. After protonation at pH below 5.0, PTX-aM assembled by a-OMPC and PTX could accelerate unload payloads. PTX-aM enhanced the cytotoxicity against PC-3 cells due to the pH-responsive drug release and the improved internalization associated with an anisamide&sigma-1 affiliation. Notably, PTX-aM retarded the tumor growth and prolonged the survival period on PC-3 tumors

xenograft-bearing mice model with a negligible systemic toxicity. As a promising biocompatible material, a-OMPC holds a promising potential to deliver PTX for anti-prostate cancer treatment.

Acknowledgements

This work was supported by the National Natural Science Foundation of China (81930099 81773664, < 81873017, 81503003), National Basic Research Program of China (2015CB755504), 111 Project from the Ministry of Education of China and the State Administration of Foreign Expert Affairs of China (No. 111-2-07, B17047), the Open Project of State Key Laboratory of Natural Medicines (No. SKLNMZZCX201811), "Double First-Class" University project (CPU2018GY47, CPU2018GF10) and the Key Medical Youth Talent Project of Jiangsu Province (QNRC2016631).

Appendix A. Supplementary data

Supplementary material related to this article can be found, in the online version, at doi:https://doi.org/10.1016/j.carbpol.2019.115498.

References

Abraham, B. G., Santala, V., Tkachenko, N. V., & Karp, M. (2014). Fluorescent protein-based FRET sensor for intracellular monitoring of redox status in bacteria at single cell level. *Analytical and Bioanalytical Chemistry, 406*(28), 7195–7204.

Allemani, C., Matsuda, T., Carlo, V. D., Harewood, R., Matz, M., Nikšić, M., et al. (2018). Global surveillance of trends in cancer survival 2000-14 (CONCORD-3): analysis of individual records for 37513025 patients diagnosed with one of 18 cancers from 322 population-based registries in 71 countries. *Lancet, 391*(10125), 1023–1075.

Almeida, E. A., Facchi, S. P., Martins, A. F., Nocchi, S., Schuquel, I. T., Nakamura, C. V., et al. (2014). Synthesis and characterization of pectin derivative with antitumor property against Caco-2 colon cancer cells. *Carbohydrate Polymers, 115*, 139–145.

Bhattarai, N., Gunn, J., & Zhang, M. (2010). Chitosan-based hydrogels for controlled, localized drug delivery. *Advanced Drug Delivery Reviews, 62*(1), 83–99.

Breunig, M., Lungwitz, U., Liebl, R., & Goepferich, A. (2006). Fluorescence resonance energy transfer: Evaluation of the intracellular stability of polyplexes. *European Journal of Pharmaceutics and Biopharmaceutics, 63*(2), 156–165.

Buschmann, M. D., Merzouki, A., Lavertu, M., Thibault, M., Jean, M., & Darras, V. (2013). Chitosans for delivery of nucleic acids. *Advanced Drug Delivery Reviews, 65*(9), 1234–1270.

Castro, F., Pinto, M. L., Silva, A. M., Pereira, C. L., Teixeira, G. Q., Gomez, L. M., et al. (2017). Pro-inflammatory chitosan/poly(γ-glutamic acid) nanoparticles modulate human antigen-presenting cells phenotype and revert their pro-invasive capacity. *Acta Biomaterialia, 63*, 96–109.

Chen, W., Wang, Y., Qin, M., Zhang, X., Zhang, Z., Sun, X., et al. (2018). Bacteria-driven hypoxia targeting for combined biotherapy and photothermal therapy. *ACS Nano, 12*(6), 5995–6005.

Chiou, W. L. (1974). Apparent volume of distribution, pulmonary clearance and bioavailability of volatile or gaseous compounds after peripheral intravenous dosing. *Research Communications in Chemical Pathology and Pharmacology, 7*(4), 679–686.

Dasargyri, A., Kümin, C. D., & Leroux, J. C. (2017). Targeting nanocarriers with anisamide: fact or artifact? *Advanced Materials, 29*(7), 1603451–1603468.

DeSantis, C. E., Lin, C. C., Mariotto, A. B., Siegel, R. L., Stein, K. D., Kramer, J. L., et al. (2014). Cancer treatment and survivorship statistics. *CA-A Cancer Journal for Clinicians, 64*(4), 252–271.

Dreifuss, T., Ben-Gal, T. S., Shamalov, K., Weiss, A., Jacob, A., Sadan, T., et al. (2018). Uptake mechanism of metabolic-targeted gold nanoparticles. *Nanomedicine (London, England), 13*(13), 1535–1549.

Durward, E., & Harris, W. J. (1998). Colorimetric method for detecting amplified nucleic acids. *Biotechniques, 25*, 608–612.

Evans, J. C., Malhotra, M., Fitzgerald, K. A., Guo, J., Cronin, M. F., Curtin, C. M., et al. (2017). Formulation and evaluation of anisamide-targeted amphiphilic cyclodextrin nanoparticles to promote therapeutic gene silencing in a 3D prostate cancer bone metastases. *Molecular Pharmaceutics, 14*(1), 42–52.

Guo, S., Lin, C. M., Xu, Z., Miao, L., Wang, Y., & Huang, L. (2014). Codelivery of cisplatin and rapamycin for enhanced anticancer therapy through synergisticeffects and microenvironment modulation. *ACS Nano, 8*(5), 4996–5009.

Huang, L., Zhao, Y., Zhang, H., Huang, K., Yang, J., & Han, G. (2017). Expanding anti-stokes shifting in triplet-Triplet annihilation upconversion for in vivo anticancer prodrug activation. *Angewandte Chemie (International Edition in English), 56*(46), 14400–14404.

Jhaveri, A., Deshpande, P., Pattni, B., & Torchilin, V. (2018). Transferrin-targeted, resveratrol-loaded liposomes for the treatment of glioblastoma. *Journal of Controlled Release, 277*, 89–101.

Jin, X., Mo, R., Ding, Y., Zheng, W., & Zhang, C. (2014). Paclitaxel-loaded *N*-octyl-*O*-sulfate chitosan micelles for superior cancer therapeutic efficacy and overcoming drug resistance. *Molecular Pharmaceutics, 11*(1), 145–157.

Katritzky, A. R., Tala, S. R., Abo-Dya, N. E., Gyanda, K., El-Gendy, B.-D., Abdel-Samii, Z. K., et al. (2009). Selective synthesis and structural elucidation of *S*-acyl- and *N*-acylcysteines. *The Journal of Organic Chemistry, 74*(18), 7165–7167.

Kimura, T., & Egawa, S. (2018). Epidemiology of prostate cancer in Asian countries. *International Journal of Urology, 25*(6), 524–531.

Li, P., Zhou, X., Qu, D., Guo, M., Fan, C., Zhou, T., et al. (2017). Preliminary study on fabrication, characterization and synergistic anti-lung cancer effects of self-assembled micelles of covalently conjugated celastrol-polyethylene glycol-ginsenosideRh2. *Drug Delivery, 24*(1), 834–845.

Li, W., Wu, J., Zhang, J., Wang, J., Xiang, D., Luo, S., et al. (2018). Puerarin-loaded PEG-PE micelles with enhanced anti-apoptotic effect and better pharmacokinetic profile. *Drug Delivery, 25*(1), 827–837.

Liu, Q., Chen, F., Hou, L., Shen, L., Zhang, X., Wang, D., et al. (2018). Nanocarrier-mediated chemo-immunotherapy arrested cancer progression and induced tumor dormancy in desmoplastic melanoma. *ACS Nano, 12*(8), 7812–7825.

Maurice, T., & Su, T. P. (2009). The pharmacology of sigma-1 receptors. *Pharmacology & Therapeutics, 124*, 195–206.

Mo, R., Jin, X., Li, N., Ju, C., Sun, M., Zhang, C., et al. (2011). The mechanism of enhancement on oral absorption of paclitaxel by *N*-octyl-*O*-sulfate chitosan micelles. *Biomaterials, 32*(20), 4609–4620.

Olivieri, M., Amata, E., Vinciguerra, S., Fiorito, J., Giurdanella, G., Drago, F., et al. (2016). Antiangiogenic effect of (±)-haloperidol metabolite II valproate ester [(±)-MRJF22] in human microvascular retinal endothelial cells. *Journal of Medicinal Chemistry, 59*(21), 9960–9966.

Qu, D., Lin, H., Zhang, N., Xue, J., & Zhang, C. (2013). In vitro evaluation on novel modified chitosan for targeted antitumor drug delivery. *Carbohydrate Polymers, 92*(1), 545–554.

Qu, D., Wang, L., Qin, Y., Guo, M., Guo, J., Huang, M., et al. (2018). Non-triggered sequential-release liposomes enhance anti-breast cancer efficacy of STS and celastrol-based microemulsion. *Biomaterials Science, 6*(12), 3284–3299.

Qu, G., Hou, S., Qu, D., Tian, C., Zhu, J., Xue, L., et al. (2019). Self-assembled micelles based on *N*-octyl-*N*'-phthalyl-*O*-phosphoryl chitosan derivative as an effective oral carrier of paclitaxel. *Carbohydrate Polymers, 207*, 428–439.

Ruetz, S., & Gros, P. (1995). Enhancement of MDR2-mediated phosphatidylcholine translocation by the bile salt taurocholate implications for hepatic bile formation. *The Journal of Biological Chemistry, 270*(43), 25388–25395.

Saari, H., Lázaro, I. E., Viitala, T., Vuorimaa, L. E., Siljander, P., & Yliperttula, M. (2015). Microvesicle- and exosome-mediated drug delivery enhances the cytotoxicity of Paclitaxel in autologous prostate cancer cells. *Journal of Controlled Release, 220*(Pt B), 727–737.

Thomas, J. D., Longen, C. G., Oyer, H. M., Chen, N., Maher, C. M., Salvino, J. M., et al. (2017). Sigma1 targeting to suppress aberrant androgen receptor signaling in prostate cancer. *Cancer Research, 77*(9), 2439–2452.

Urandur, S., Banala, V. T., Shukla, R. P., Mittapelly, N., Pandey, G., Kalleti, N., et al. (2018). Anisamide-anchored lyotropic nano-liquid crystalline particles with AIE effect: A smart optical beacon for tumor imaging and therapy. *ACS Applied Materials & Interfaces, 10*(15), 12960–12974.

Wang, H., Zhu, W., Liu, J., Dong, Z., & Liu, Z. (2018). pH-responsive nanoscale covalent organic polymers as a biodegradable drug carrier for combined photodynamic chemotherapy of cancer. *ACS Applied Materials & Interfaces, 10*(17), 14475–14482.

Wang, L., Pei, J., Cong, Z., Zou, Y., Sun, T., Davitt, F., et al. (2019). Development of anisamide-targeted PEGylated gold nanorods to deliver epirubicin for chemo-photothermal therapy in tumor-bearing mice. *International Journal of Nanomedicine, 8*(14), 1817–1833.

Wu, Y., Zhang, L., Na, R., Xu, J., Xiong, Z., Zhang, N., et al. (2015). Plasma genistein and risk of prostate cancer in Chinese population. *International Urology and Nephrology, 47*(6), 965–970.

Yang, D., Comeau, A., Bowen, W. D., Mach, R. H., Ross, B. D., Hong, H., et al. (2017). Design and investigation of a [18F]-labeled benzamide derivative as a high affinity dual sigma receptor subtype radioligand for prostate tumor imaging. *Molecular Pharmaceutics, 14*(3), 770–780.

Yang, R., Mondal, G., Wen, D., & Mahato, R. I. (2017). Combination therapy of paclitaxel and cyclopamine polymer-drug conjugates to treat advanced prostate cancer. *Nanomedicine, 13*(2), 391–401.

Zamaleeva, A. I., Despras, G., Luccardini, C., Collot, M., de Waard, M., Oheim, M., et al. (2015). FRET-based nanobiosensors for imaging intracellular Ca^{2+} and H^{+} microdomains. *Sensors (Basel), 15*(9), 24662–24680.

Zhang, A. L., & Russell, P. J. (2006). Paclitaxel suppresses the growth of primary prostate tumours (RM-1) and metastases in the lung in C57BL/6 mice. *Cancer Letters, 233*(1), 185–191.

Zhang, N., Xu, X., Zhang, X., Qu, D., Xue, L., Mo, R., et al. (2016). Nanocomposite hydrogel incorporating gold nanorods and paclitaxel-loaded chitosan micelles for combination photothermal-chemotherapy. *International Journal of Pharmaceutics, 497*(1–2), 210–221.

Zhou, L., Jing, Y., Liu, Y., Liu, Z., Gao, D., Chen, H., et al. (2018). Mesoporous carbon nanospheres as a multifunctional carrier for cancer theranostics. *Theranostics, 8*(3), 663–675.